AD-A019 500

NUMERICAL COMPUTATION OF TURBULENT SHEAR FLOWS

Steven A. Orszag, et al

Flow Research, Incorporated

Prepared for:

Office of the Secretary of Transportation

July 1973

FLOW RESEARCH REPORT No. 19

NUMERICAL COMPUTATION OF TURBULENT SHEAR FLOWS*

STEVEN A. ORSZAG AND YIH-HO PAO

JULY, 1973

FLOW RESEARCH, INC.
1819 S. CENTRAL AVE.
KENT, WASH. 98031
(206) 854-1370, 854-9590

*This work is supported by Fluid Dynamics Branch, Office of Naval Research under Navy Contract No. N00014-72-C-0355, ONR Task No. NR 062-464. A portion of the research fund was provided by the Climative Impact Assessment Program (CIAP), Department of Transportation (DOT-AS-30041). This work was presented at the Second IUGG-IUTAM Symposium on Turbulent Diffusion in Environmental Pollution 8-14, April 1973, Charlottesville, Va. It will appear in Advances in Geophysics.

Technical Report Documentation Page

1. Report No.	2. Government Accession No.	3. Recipient's Catalog No.
DOT-TST-74-27		

4. Title and Subtitle
Numerical Computation of Turbulent Shear Flows

5. Report Date
July 1973

6. Performing Organization Code

8. Performing Organization Report No.
19

7. Author(s)
Steven A. Orszag and Yih-Ho Pao

9. Performing Organization Name and Address
Flow Research, Inc.
1819 S. Central Avenue
Kent, Washington 98031

10. Work Unit No. (TRAIS)

11. Contract or Grant No.
DOT-AS-30041

13. Type of Report and Period Covered
Final Report

12. Sponsoring Agency Name and Address
Office of the Secretary
Department of Transportation
Washington, DC 20590

14. Sponsoring Agency Code

15. Supplementary Notes

16. Abstract

In this paper, we report simulations of turbulent shear flows by numerical solution of the three-dimensional Navier-Stokes equations. This approach provides several advantages over more conventional approaches. First, the complete flow field is obtained at all times so that detailed flow characteristics may be obtained that would be difficult to measure in the laboratory. Second, initial conditions can be accurately controlled so that their effect may be determined. Third, numerical simulations are convenient experiments to assess the effect of various physical processes, like chemical reactions, on turbulence and vice versa. Fourth, the simulations results can be used to test and suggest various statistical hypotheses involved in turbulence models and theories.

17. Key Words	18. Distribution Statement
Atmospheric models, Turbulence, Shear flow.	Document is available to the public through the National Technical Information Service, Springfield, Virginia 22151

19. Security Classif. (of this report)	20. Security Classif. (of this page)	21. No. of Pages	22. Price
Unclassified	Unclassified	19	

Form DOT F 1700.7 (8-72) Reproduction of completed page authorized

1. Introduction

In this paper, we report simulations of turbulent shear flows by numerical solution of the three-dimensional Navier-Stokes equations. This approach provides several advantages over more conventional approaches. First, the complete flow field is obtained at all times so that detailed flow characteristics may be obtained that would be difficult to measure in the laboratory. Second, initial conditions can be accurately controlled so that their effect may be determined. Third, numerical simulations are convenient experiments to assess the effect of various physical processes, like chemical reactions, on turbulence and vice versa. Fourth, the simulations results can be used to test and suggest various statistical hypotheses involved in turbulence models and theories.

The present work is an extension to inhomogeneous shear flows of the three-dimensional, homogeneous, isotropic turbulence simulations reported by Orszag & Patterson (1972). In this earlier work, simulations using up to $(32)^3$ Fourier modes to represent each velocity component were performed at microscale Reynolds number 20-50 (grid Reynolds numbers 5000-3000), corresponding to moderate Reynolds number grid turbulence. The results of these homogeneous turbulence simulations agreed well with both turbulence theory (e.g., the direct interaction approximation) and laboratory experiments. Simulations have also been made of two-dimensional 'turbulence' using up to $(128)^2$ Fourier modes (Herring et al 1973) with successful comparisons with the results of turbulence theories. These successful simulations gave impetus to the present extension to shear flows.

In the homogeneous turbulence simulations, it was observed that some important features of the flows were Reynolds number independent (Herring et al 1973), so that there is basis for assuming that the large-scale features of flows simulated at huge Reynolds numbers. It is also reasonable to assume Reynolds-number-independence of large scales in shear flows provided initial and boundary conditions are Reynolds number independent. It seems that Reynolds number dependencies observed in laboratory flows may be ascribed to variations in initial or boundary conditions; for example, Reynolds number variations in turbulent jets seem to be mainly due to variations in inlet conditions (like boundary layer thickness) with Reynolds number.

As a first application of our shear flow turbulence codes, we have simulated the momentumless wake of a self-propelled body. As pointed out by Naudascher (1965), the momentumless wake bears close relationship to grid-generated homogeneous turbulence, since both are characterized by a very limited region in which there is significant energy transfer from mean flow to turbulence through Reynolds stresses.

In Sec. 2, we summarize the dynamical equations and boundary conditions employed with particular emphasis on the momentumless wake model. In Sec. 3, some novel aspects of the numerical approximation are discussed, while in Sec. 4, some results are presented for wake turbulence. Finally in Sec. 5, we summarize our results and future outlook.

2. Equation of Motion

The Navier-Stokes equations of motion for an imcompressible fluid are

$$\frac{\partial \underset{\sim}{v}(\underset{\sim}{x},t)}{\partial t} = \underset{\sim}{v}(\underset{\sim}{x},t)\times\underset{\sim}{\omega}(\underset{\sim}{x},t) - \underset{\sim}{\nabla}\pi(\underset{\sim}{x},t) + \nu\nabla^2\underset{\sim}{v}(\underset{\sim}{x},t)$$

$$\underset{\sim}{\nabla}\cdot\underset{\sim}{v}(\underset{\sim}{x},t) = 0$$

where $\underline{y}(\underline{x},t)$ is the three-dimensional velocity field, $\underline{\omega}(\underline{x},t)=\underline{\nabla} \times \underline{y}(\underline{x},t)$ is the vorticity, $\pi(\underline{x},t) = p + \frac{1}{2} v^2$ is the pressure head, $p(x,t)$ is the pressure, and ν is the kinematic viscosity. Eq. (1) is written in rotation form to facilitate numerical solution (Sec. 3).

Boundary conditions require more discussion. In order to simulate the momentumless wake of a self-propelled body the computational domain should include a sizeable region of potential flow both upstream and downstream of the body as large as the body itself. However, this would be very wasteful where most of the computational degrees of freedom would be involved in resolving the flow outside the turbulent wake. Even within the wake, the first several body diameters downstream are of adjustment to more self-similar conditions downstream. The resolution problem is a serious one. Presently practicable numerical simulations involve at most order of 10^5 degrees of freedom to describe the velocity field, there would remain little more than 10^3 degrees of freedom to do the flow in the turbulent wake. Clearly, it is not possible to simulate details of a turbulent flow with so little resolution.

In order to avoid the resolution problem just described, we simulate wake flow in the following way. We isolate a slab in a momentumless turbulent wake (Fig. 1) and follow its time evolution by considering it enclosed in a three-dimensional box as shown in Fig. 2. The wake axis is assumed to be along the x_1 - axis and periodic boundary conditions are applied at $x_1 = 0, L_1$ and $x_2 = 0, L_2$. On the other hand, regid free-slip (no stress) or rigid no-slip boundary conditions are applied at $x_3 = 0, L_3$. This choice of boundary conditions in the x_3- direction is necessitated by the face that our computer codes are written to solve also the Boussinesq equation of motion of a stratified fluid for which the x_3-direction is singled as the direction of gravity and the equations of shear flow in a channel with rigid

top and bottom boundaries.

Initial conditions are chosen so that the slab of turbulence is a realization of a section of a fully developed turbulent wake, i.e.

$$\underset{\sim}{v}(\underset{\sim}{x},0) = \bar{\underset{\sim}{v}}(\underset{\sim}{x},0) + \underset{\sim}{v}'(\underset{\sim}{x},0) \tag{3}$$

Here the mean defect velocity $\bar{\underset{\sim}{v}}(\underset{\sim}{x},0)$ is chosen to be

$$\bar{\underset{\sim}{v}}(\underset{\sim}{x},0) = v_d(r)\,\hat{x}_1 \tag{4}$$

where $\hat{x}_1$ is the unit vector in the x_1-direction, $r^2 = (x_2-\frac{1}{2}L_2)^2 + (x_3-\frac{1}{2}L_3)^2$ and

$$\int_0^\infty v_d(r) r\, dr = 0$$

in order to simulate the momentumless wake. The initial fluctuating velocity $\underset{\sim}{v}'(\underset{\sim}{x},0)$ is chosen as a realization of an incompressible random velocity field with specified local energy spectrum and turbulence. Some of the details involved in the construction of $\underset{\sim}{v}'$ are explained in Sec. 3.

Numerical solution of the Navier-Stokes equations from the imposed initial conditions gives the time evolution of the simulated cylindrical section of turbulence. After evolution time t, the results are interpreted as a realization of a section of the wake flow at a distance $x_1 = U_0 t$ downstream from the location of the initial wake section, where U_0 is the body velocity. In other words, the initial flow is chosen to have the same (or rather similar) statistical properties as a section of a turbulent wake and the time evolution of the flow is interpreted as the downstream variation of the wake. The model we solve numerically is statistically homogeneous along the wake axis x_1 but nonstationary in time; the wake in the frame of a uniformly moving body is statistically stationary in time but is inhomogeneous in x_1. It is asserted that the Galilean transformation $x_1 = U_0 t$ relates the

numerical and physical experiments.

3. Numerical Methods

3.1 Free-slip boundaries

If the boundary conditions at $x_3 = 0, L_3$ are no-stress (free-slip) while those at $x_1 = 0, L_1$ and $x_2 = 0, L_2$ are periodic then

$$\frac{\partial v_1}{\partial x_3} = \frac{\partial v_2}{\partial x_3} = v_3 \text{ on } x_3 = 0, L_3; \; \underset{\sim}{v}(x_1 + mL_1, x_2 + nL_2, x_3) = \underset{\sim}{v}(\underset{\sim}{x}) \qquad (6)$$

In this case, the velocity field can be expanded in the Fourier series

$$v_\alpha(\underset{\sim}{x},t) = \sum_{|k_1|<K_1} \sum_{|k_2|<K_2} \sum_{0 \le k_3 < K_3} u_\alpha(\underset{\sim}{k},t) \exp[2\pi i(k_1 x_1/L_1 + k_2 x_2/L_2)]$$

$$\cdot \begin{cases} \cos \pi k_3 x_3/L_3, & \alpha = 1,2 \\ \sin \pi k_3 x_3/L_3, & \alpha = 3 \end{cases} \qquad (7)$$

where the indicated summations are over integer k_1, k_2, k_3. For the simulations reported below, the cutoffs are chosen as $K_1 = K_2 = 16$, $K_3 = 32$, so that the spectral representations (7) each involve about $(32)^3$ independent degrees of freedom (Fourier amplitudes).

We have used the expansions (7) in two kinds of numerical approximation to the Navier-Stokes equations. In the spectral method (Orszag 1971a), equations for $\underset{\sim}{u}(\underset{\sim}{k})$ are derived by substituting (7) into (1), multiplying the result by $\exp[-2\pi i(k_1 x_1/L_1 + k_2 x_2/L_2)]\cos[\pi k_3 x_3/L_3]$ for $\alpha = 1, 2$ (and by the same expression with the cosine replaced by sine if $\alpha = 3$), and finally integrating the result over the box $0 \le x_\alpha < L_\alpha$. The resulting equations are, after elimination of the pressure by means of the incompressibility constraint (2),

$$\frac{\partial \bar{u}_\alpha(\underset{\sim}{k},t)}{\partial t} + \nu \bar{k}^2 \bar{u}_\alpha(\underset{\sim}{k},t) = -i\bar{k}_\beta(\delta_{\alpha\gamma} - \bar{k}_\alpha \bar{k}_\gamma/\bar{k}^2) \sum_{\substack{\underset{\sim}{p}+\underset{\sim}{q}=\underset{\sim}{k} \\ -K_\rho < p_\rho,\ q_\rho < K_\rho}} \bar{u}_\beta(\underset{\sim}{p},t)\bar{u}_\gamma(\underset{\sim}{q},t) \tag{8}$$

where $\bar{k}_\alpha = 2\pi k_\alpha/L_\alpha$ for $\alpha = 1,2$ and $\bar{k}_3 = \pi k_3/L_3$, and

$$\bar{u}_\alpha(\underset{\sim}{k},t) = \begin{cases} \frac{1}{2} u_\alpha(k_1,k_2,|k_3|,t), & \alpha = 1,2 \\ \frac{1}{2i} \operatorname{sgn} k_3 u_3(k_1,k_2,|k_3|,t), & \alpha = 3 \end{cases} \tag{9}$$

Numerical solution of (8) is accomplished using fast Fourier transform methods to evaluate the convolution sums, leapfrog time differencing on the nonlinear terms, and Crank-Nicolson (implicit) time differencing on the viscous terms. Overall, 18 Fourier transforms on $(32)^3$ points must be performed each time step (Orszag 1971a).

In the pseudospectral method (Fox and Orszag 1973), the expansions (7) are used as an interpolatory tool to evaluate the derivatives appearing in (1). "Grid" points $x_\alpha = L_\alpha j_\alpha/2K_\alpha$, $j_\alpha = 0, \ldots, 2K - 1$ for $\alpha = 1,2$, $x_3 = L_3 j_3/K_3$. $j_3 = 0, \ldots, K_3$ are introduced and the series (7) are used to evaluate derivatives as, for example,

$$\omega_3(\underset{\sim}{x},t) = \sum_{|k_1|<K_1} \sum_{|k_2|<K_2} \sum_{0\le k_3<K_3} [i\bar{k}_1 u_2(\underset{\sim}{k},t) - i\bar{k}_2 u_1(\underset{\sim}{k},t)] \cdot \exp[i\bar{k}_1 x_1 + i\bar{k}_2 x_2] \cos \bar{k}_3 x_3 \tag{10}$$

The final result of this procedure is to give a set of equations for the spectral amplitudes $\bar{u}(\underset{\sim}{k})$, defined by (9), that are identical to (8) except for the replacement of the convolution sums by similarly truncated sums with $p_\alpha + q_\alpha = k_\alpha \pm 2K$ or $p_\alpha + q_\alpha = k_\alpha$ (Orszag 1971a). The additional terms entering the sums in (8) are usually called "aliasing" terms. It has been shown (Fox and Orszag 1973) that the differences in the results obtained by the present pseudospectral method and the spectral method are generally negligible so long as either method gives an accurate solution of the equations of motion. Since the pseudospectral method may be implemented in only 9

Fourier transforms over $(32)^3$ points per time step, it is roughly a factor 2 more efficient than the spectral method and so has been used for most of the simulations reported below.

Both the spectral and pseudospectral methods have been programmed for a CDC 7600. The programs involve double buffering of data between small core memory, large core memory, and disks. The spectral method requires about 6 s per time step on the CDC 7600, while the pseudospectral code requires only 3.2 s per time step, both for the cutoffs $K_1 = K_2 = 16$, $K_3 = 32$. Many of the critical internal loops of the program are written in assembly language to avoid inefficiencies attributable to the Fortran compiler, although further improvements in the code should permit a speedup of nearly 50%.

Besides the speed advantage of the pseudospectral method over the spectral method, the former has the great advantage that it applies with but the most minor of modifications to problems involving more complicated physics, like chemical reactions or radiation. Since the expansions (7) are used merely as an interpolatory tool in the evaluation of derivatives, they may be similarly used in the evaluation of these more complicated effects. Nevertheless, the pseudospectral method shares all the advantages of the spectral method with regard to accuracy and, especially, efficiency improvement over finite-difference schemes (Orszag & Israeli 1974). The expression of (1) in rotation form is useful since it gives pointwise energy conservation.

3.2 No-slip boundaries

With no-slip boundary conditions applied at $x_3 = 0, L_3$, the velocity satisfies

$$\underset{\sim}{v} = 0 \text{ on } x_3 = 0, L_3, \quad \underset{\sim}{v}(x_1 \pm mL_1, x_2 \pm nL_2, x_3) = \underset{\sim}{v}(\underset{\sim}{x}) \tag{11}$$

instead of (6). It is no longer appropriate to use the Fourier expansions (7), not just because $v_1 = v_2 = 0$ at $x_3 = 0, L_3$, but rather because imposition

of a Fourier series representation of the x_3 dependence would induce Gibbs phenomena at the boundaries and result in slow convergence of the Fourier series (Orszag 1971a).

No-slip boundaries are best treated by Chebyshev expansion in x_3, (Orszag 1971b). The velocity field is represented as

$$\underset{\sim}{v}(\underset{\sim}{x},t) = \sum_{|k_1|<K_1} \sum_{|k_2|<K_2} \sum_{0\le k_3<K_3} \underset{\sim}{u}(\underset{\sim}{k},t) \exp[i\underset{\sim}{k}_1 x_1 + ik_2 x_2] T_{k_3}([2x_3 - L_3]/L_3) \tag{12}$$

where the nth degree Chebyshev polynomial $T_n(x)$ is defined by $T_n(\cos\theta) = \cos n\theta$. It may be shown that, if $\underset{\sim}{v}(\underset{\sim}{x})$ is smooth, the series (12) or any of its termwise derivatives do not exhibit Gibbs phenomena at the boundaries. Equivalently, the series (12) converges faster than algebraically as $K_\alpha \to \infty$. Notice that the boundary conditions (11) must be imposed as constraints on (12).

One advantage of (12) is that it leads to pseudospectral approximations to (1), (2) that are very similar in form to that following from the Fourier series (7). In particular, the pseudospectral equations with (12) may be implemented in 9 Fourier transforms per time step, and are but slightly less efficient than for free-slip boundaries. With cutoffs $K_1 = K_2 = 16$ and $K_3 = 32$, our code requires 4 s per time step. In this latter code, time differencing is done by Adams-Bashforth differencing (Lilly 1965) on the nonlinear terms (to avoid instability that would result from use of leapfrog because of the stability induced by the boundary conditions) and Crank-Nicolson on the viscous terms. The pressure computation is done by using (2) to get an equation tridiagonal in the Chebyshev index k_3 for the pressure and diagonal in k_1 and k_2. Solution of the resulting tridiagonal system accounts for most of the additional time required by the rigid boundary code over the free-slip

ndary code.

Methods based on the spectral expansion (12) have an important advantage over difference methods, in addition to the advantages they enjoy when periodic of free-slip boundary conditions are applied. The "grid" points for the pseudospectral method based on (12) are $x_3 = \frac{1}{2} L_3 (1 + \cos \pi j_3/K_3)$ for $j_3 = 0, \ldots, K_3$, so that the effective resolution near the walls $x_3 = 0, L_3$ is $\Delta x_3 \sim L_3/K_3^2$. In fact, if there is a boundary layer of thickness δ along either $x_3 = 0$ or $x_3 = L_3$, it may be shown (Orszag & Israeli 1974) that it is sufficient to take $K_3 \sim 3(L_3/\delta)^{1/2}$ to achieve better than 1% accuracy in the boundary layer. In effect, the Chebyshev polynomial expansion gives a highly nonuniform grid near the boundaries. This behavior is particularly appropriate for the study of channel flows, etc. where thin boundary layer are apt to develop.

3.3 Initial condicions

In the wake model introduced in Sec. 2, initial conditions of the form of a "cylinder" of turbulence are required. The mean defect velocity (4) may be imposed arbitrarily, but the fluctuating component $\underset{\sim}{v}'(\underset{\sim}{x})$ must satisfy the incompressibility constraint. This is done by writing

$$\underset{\sim}{v}'(\underset{\sim}{x}) = \underset{\sim}{\nabla} \times \underset{\sim}{A}'(\underset{\sim}{x}) \tag{13}$$

where the vector potential $\underset{\sim}{A}'(\underset{\sim}{x})$ is chosen to achieve the desired local energy spectrum and turbulence intensity. It suffices to choose $\underset{\sim}{A}'(\underset{\sim}{x})$ to be of the form

$$\underset{\sim}{A}'(\underset{\sim}{x}) = [I(r)]^{\frac{1}{2}} \underset{\sim}{B}(\underset{\sim}{x}) \tag{14}$$

where the turbulence intensity function I(r) is a nonrandom function of only the distance from the wake axis x_1 and the fluctuation component B(x) is chosen as a realization of a homogeneous, isotropic random field with specified isotropic energy spectrum, as done by Orszag & Patterson (1972). If

the intensity function is chosen to vanish outside a radius r_0 from the wake axis, the resulting turbulent velocity field is, by (13), nonturbulent outside the cylinder of radius r_0 centered on the wake axis.

In summary, our technique of imposing the initial conditions allow arbitrary mean velocity profile, turbulence intensity profile, and local turbulence energy spectrum.

4. Momentumless Wake

The wake model of Sec. 2 and the numerical methods of Sec. 3 permit simulation of the turbulent wake of a self-propelled body. Free-slip boundary conditions are applied at $x_3 = 0$, L_3 and the spectral cutoffs $K_1 = K_2 = K_{16}$, $K_3 = 32$ are used. The following choice of initial parameters was made: $L_1 = L_2 = L_3 = 2$, $v_d(r) = v_0 \sin(r/r_1)/(r/r_1)$ where $r_1 = 1/4$, $I(r) = \max[1-r^2/4.5,0]$, and turbulence energy spectrum $E(k) - Ak^4\exp(-Bk^2)$ [cf. Orszag & Patterson 1972]. The initial conditions are chosen to match as closely as possible the results of Naudascher (1965) and Wang (1965) at a location 4 body diameters behind a self-propelled disk in a wind tunnel. In the numerical simulations, the viscosity is chosen to be $\nu = .005$, so that the Reynolds number of the simulation is roughly 13,000 (run 2a), and $\nu = .003$ with Reynolds number roughly 22,000 (run 3). In comparison, the laboratory experiments of Naudascher and Wang were run at Reynolds numbers of roughly 55,000.

Some measure of the degree of complication of the flow that is simulated is given by Figs. 3&4. In Fig. 3, contours of the run 3 axial mean velocity are plotted at $t = .8$, corresponding, to about 7 diameters downstream from the body upon making identification of body velocity by the ratio $\max[v_d(r)]/U_o$ at the station at $x/D = 4$ with the experimental results. The axial mean is

determined by averaging over the x_1-direction. In Fig. 4, contours of the run 3 x_1-component of vorticity are plotted at t = .8.

In Fig. 5, we compare the axial variation of maximum turbulent intensity with the results of Wang and Naudascher. Here U_0 and t_0 are determined as explained above by correspondence with the data at the station at x = 4D, while x_0 = 2D according to Naudascher and Wang. It is apparent from these results that the present simulations are in substantial agreement with the laboratory results of Naudascher and Wang, at least over the limited downstream range of the present experiments.

In Fig. 6, we compare the radial variation of axial mean-square turbulent intensity in the laboratory experiments and the numerical calculations. The curve labelled t = 0 shows the initial distribution, while that labelled t = .522 shows the resulting distribution for run 2a at about 6D downstream from the body. Again, the agreement with the experimental results is satisfactory.

It is apparent from the simulation results of this section that numerical simulation of turbulent shear flows is well within present computational capabilities. However, the process of extracting useful information about shear flows from numerical simulations is still in its infancy. The most significant problem with the present simulations is the scarcity of points in the axial direction with which to compute averages. With just 32 points in the longitudinal direction, statistical errors are more large and either multi-time step information or ensembles must be employed to improve the statistics. This situation should be contrasted with the case for homogeneous, isotropic turbulence where space averages suffice to give statistical results generally to within 5% (Orszag & Patterson 1972).

5. Conclusions

The present simulations of turbulent shear flows are but a first step toward proper understanding of the basic mechanisms and dynamics of these flows. Detailed comparisons and tests are presently being made between various turbulence modelling hypotheses, laboratory experiments, and the present simulations. As time and the art of numerical simulation progress, simulations like the present ones should be expected to fulfill more and more the need of a laboratory workhorse. Out present simulations provide ample evidence for this. The computer codes we have written and sufficiently general to study channel flows like plane Poiseuille and plane Couette flows, as well as momentumless and momentumfull wakes, both in homogeneous and stratified fluids. Experimental set-up of this variety of shear flows, notwithstanding specifying the form of the shear and turbulence profiles that may be imposed, would be a herculean task. On the other hand, the computer simulations can handle all these cases.

In future work on the momentumless wake, we shall report on longer simulation runs now underway and on techniques to improve the statistics of the results. In order to improve the choice of initial conditions, simulations runs are made in which the pseudorandom initial conditions imposed as described in Sec. 3.3 are let to evolve for about 10 body diameters downstream and then are reapplied, amplified in excitation, at a virtual upstream point in order to begin the calculation anew. This approach avoids the difficulty of modelling imprecisely known laboratory experiments. With the initial conditions imposed as in Sec. 3.3, the wake is very sensitive to the initial turbulence level relative to the mean shear, while much of this dependence is avoided by the present technique.

REFERENCES

Fox, D. G. and Orszag, S. A. (1973). J. Comp. Phys. 11, 612-619.

Herring, J. R., Orszag, S. A., Kraichnan, R. H., and Fox, D. G. (1973). "Decay of Two-Dimensional Homogeneous Turbulence." To appear in J. Fluid Mech.

Lilly, D. K. (1965). Mon. Weath. Rev. 93, 11-26.

Naudascher, E. (1965). J. Fluid Mech. 22, 625-656.

Orszag, S. A. (1971a). Stud. in Appl. Math. 50, 293-327.

Orszag, S. A. (1971b). Phys. Rev. Letters 26, 1100-1103.

Orszag, S. A. and Israeli, M. (1974). Ann. Rev. Fluid Mech. 6, xxx.

Orszag, S. A. and Patterson, G. S. (1972). Phys. Rev. Letters 28, 76-79.

Wang, H. (1965). Ph.D. Thesis, Univ. of Iowa.

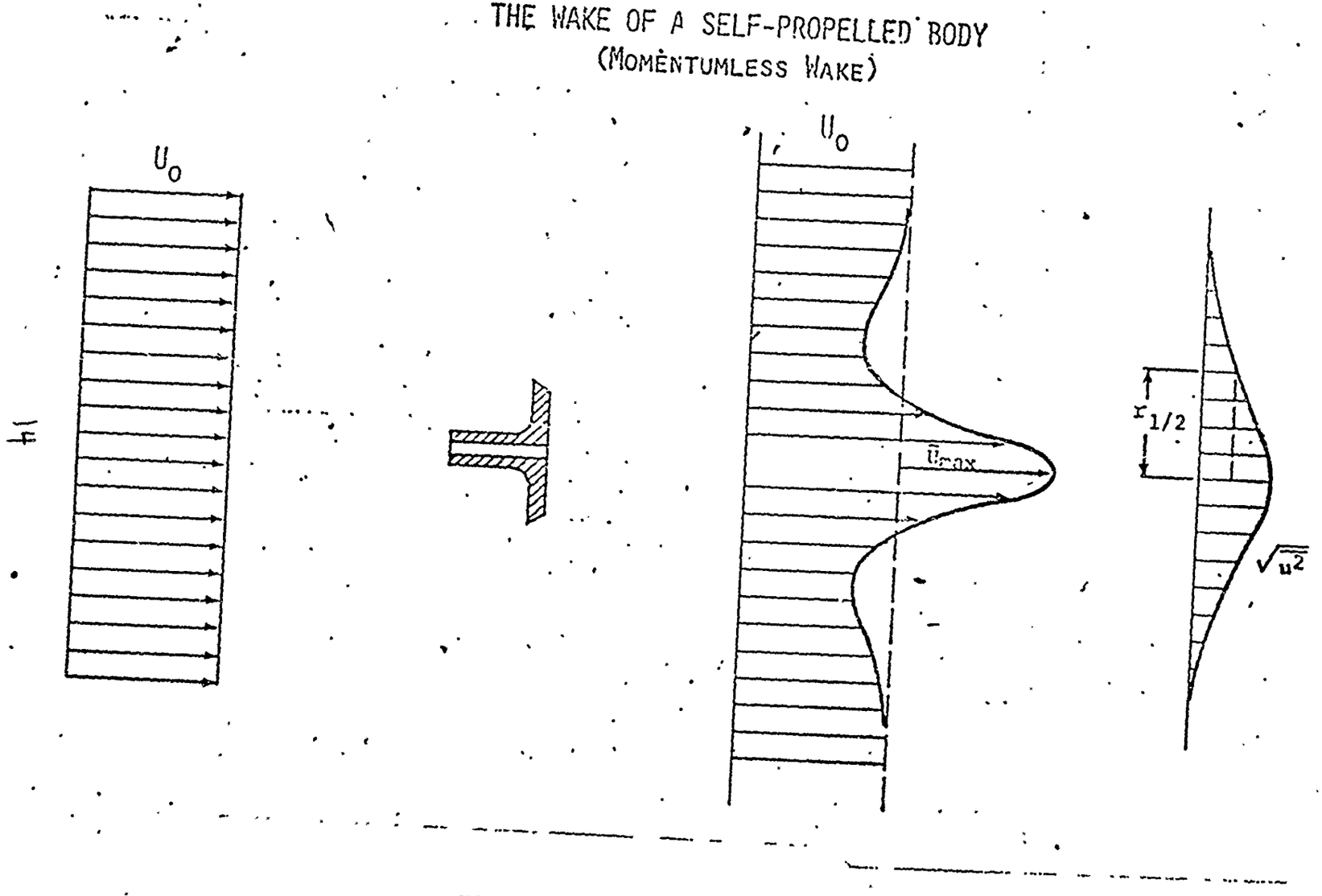

Fig. 1. A Momentumless Turbulent Wake

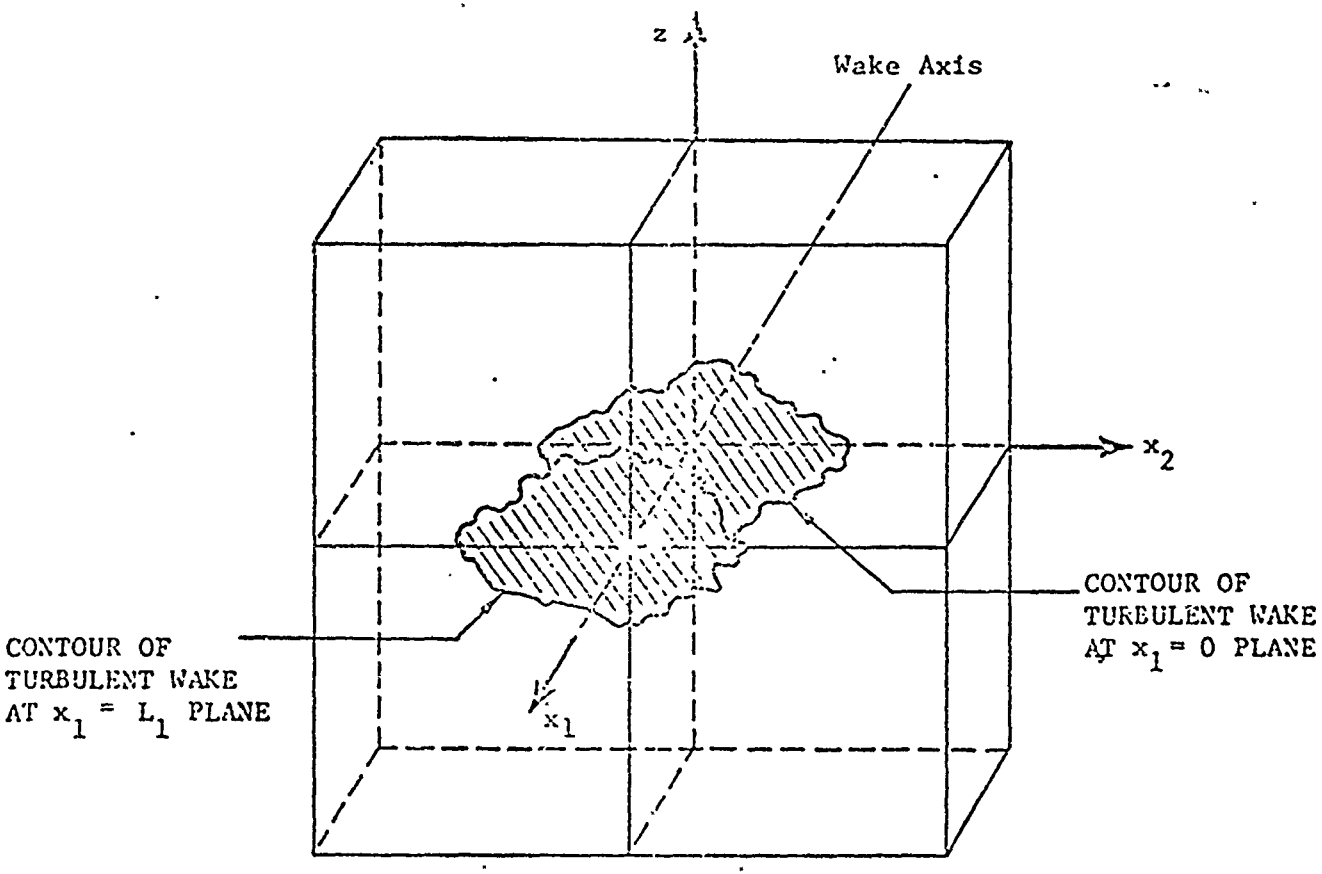

Fig. 2 Spatial box enclosing the section of wake $(0, L_1)$ is in Fig. 1. Periodic boundary conditions are applied at the sidewalls and either free-slip or no-slip conditions are applied at the top and bottom.

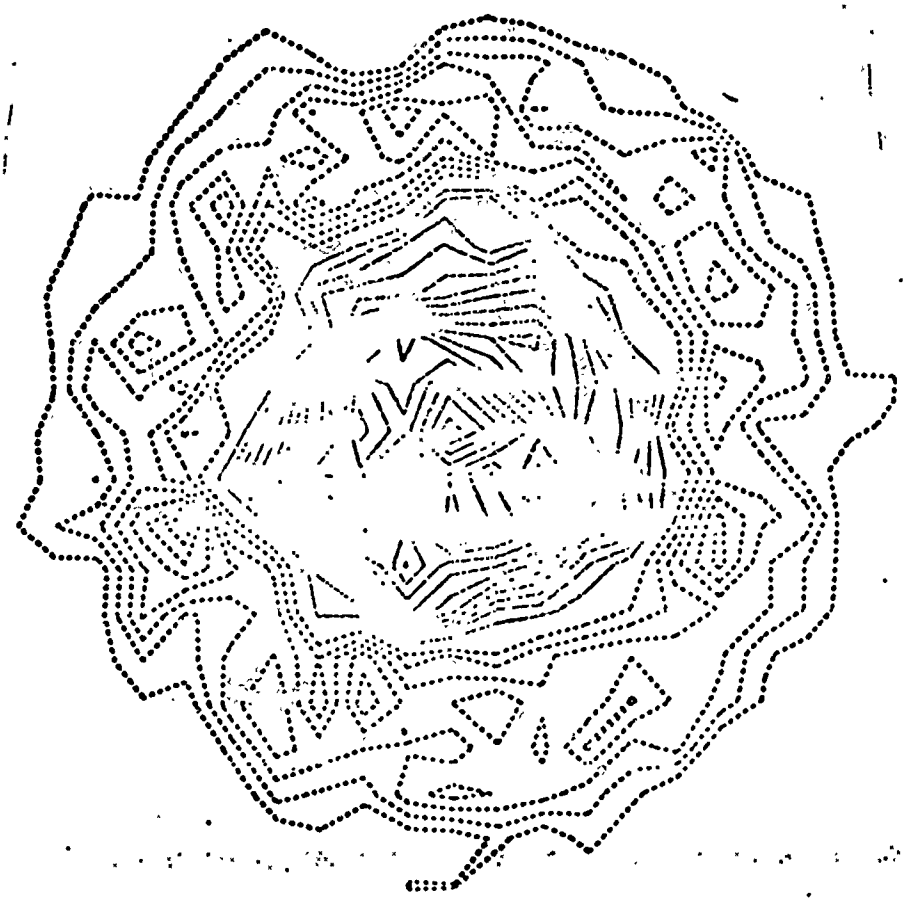

Fig. 3 Axial mean velocity contours for run 3 at t = .8.

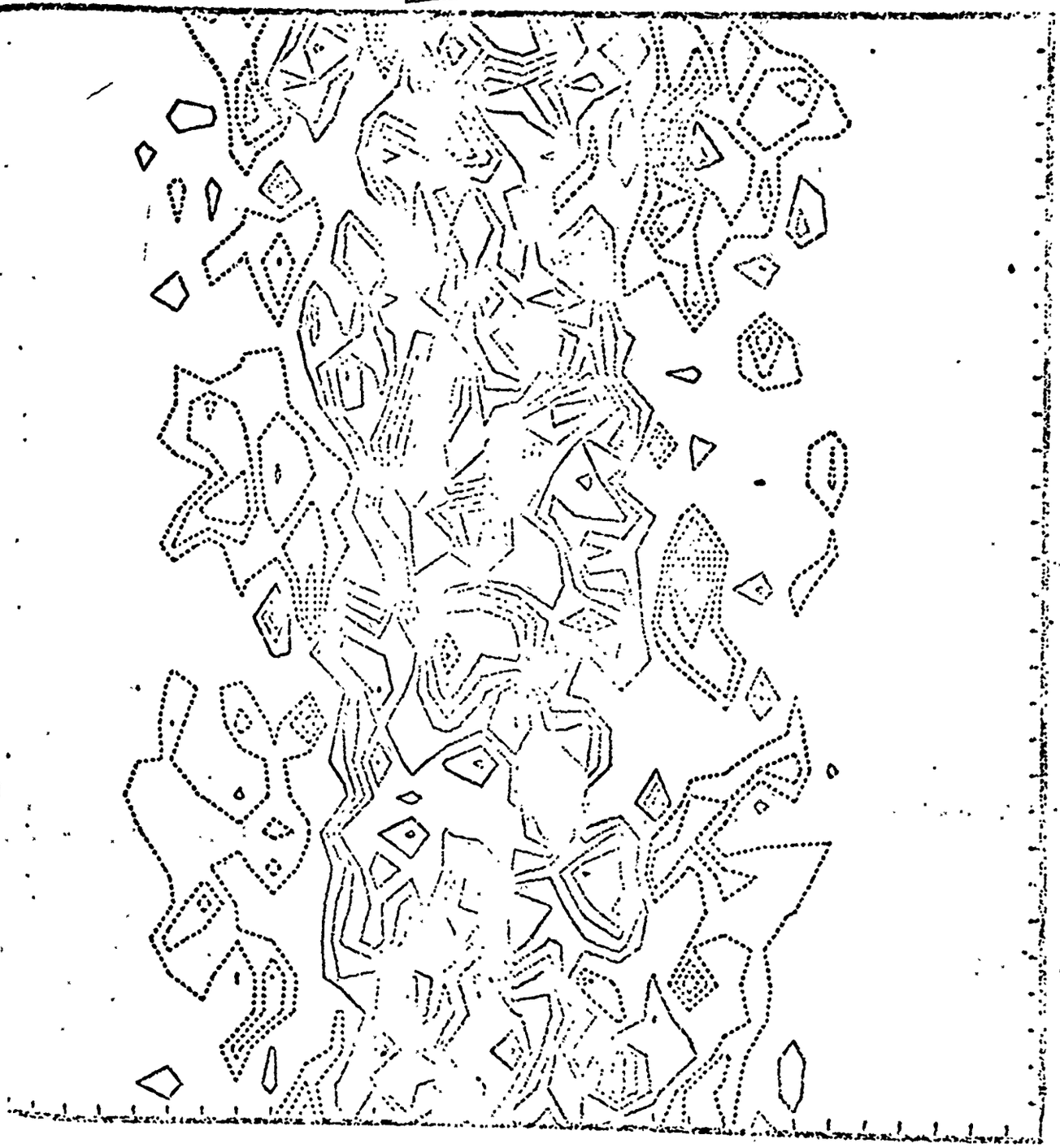

Fig. 4 Axial component of vorticity contours for run 3 at t = .8

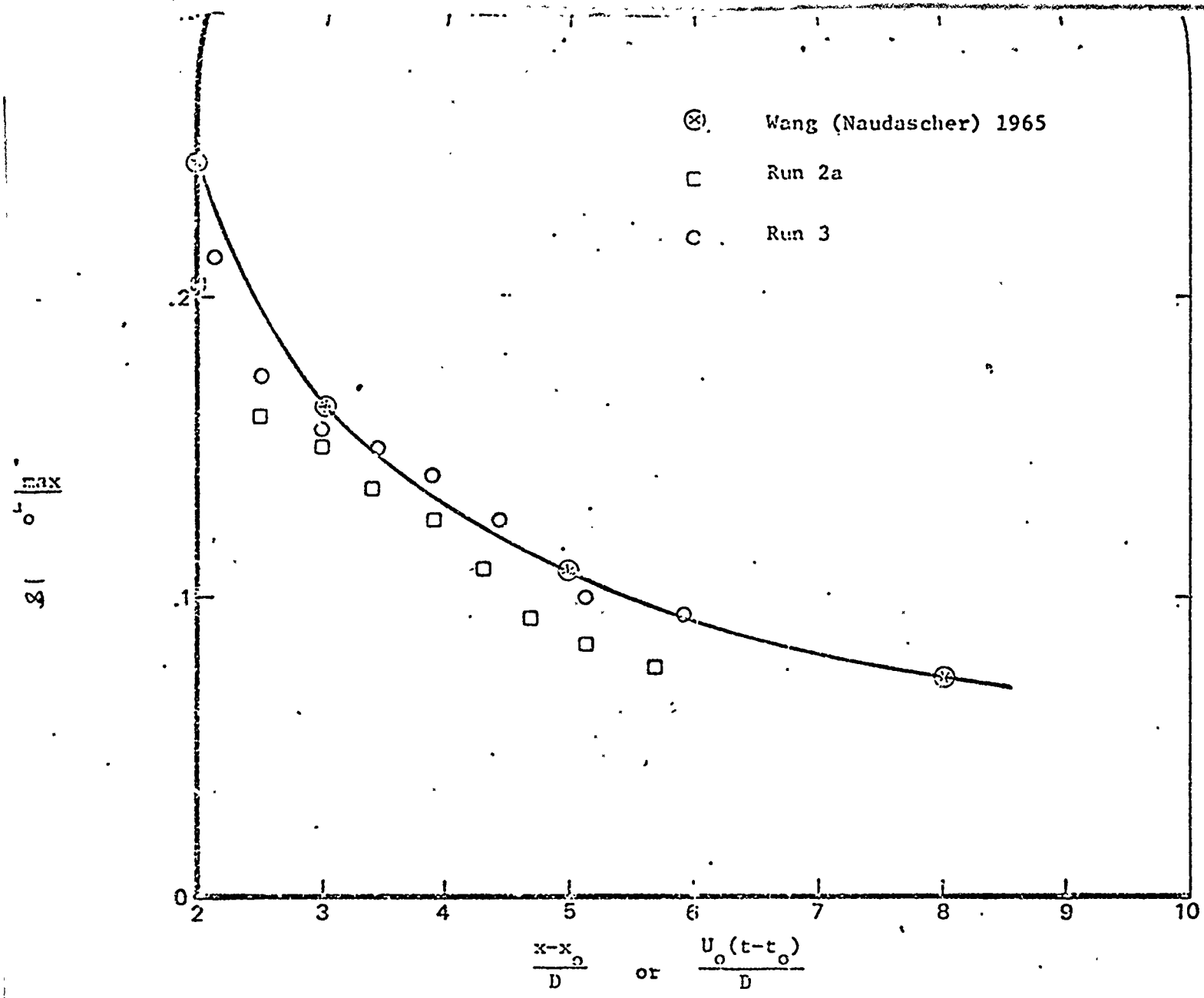

Fig. 5 . Axial variation of maximum turbulent intensity.
Cross circles: results of Wang and Naudascher.
Squares: Run 2 Circles: Run 3.

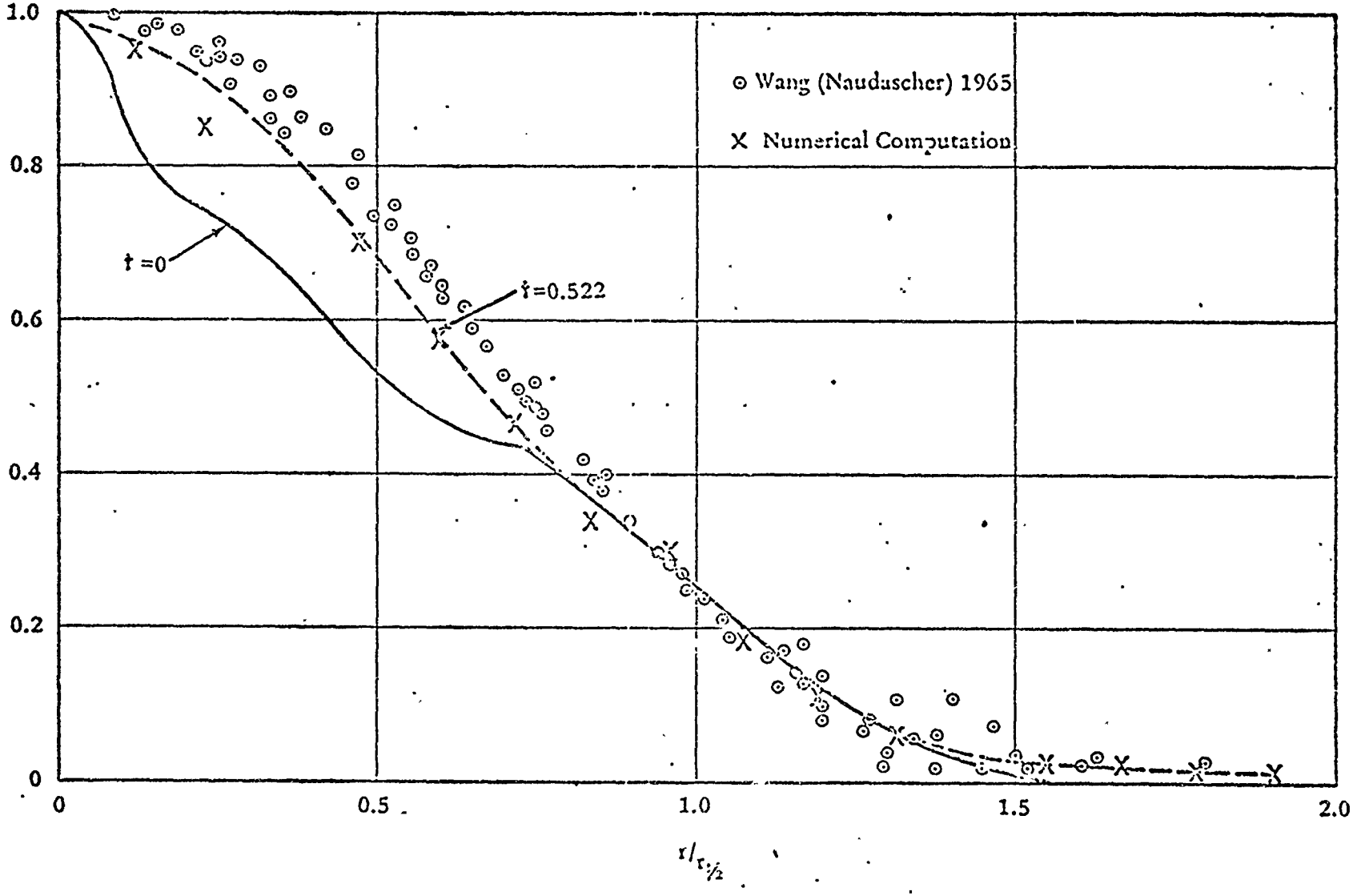

Fig. 6 Radial variation of axial mean-square turbulent into at t = .522 for run 2a. Crosses: run 2a. Circles: results of Wang and Naudascher.